INTERNATIONAL JOURNAL FOR NUMERICAL METHODS IN FLUIDS
Int. J. Numer. Meth. Fluids 2005; **48**:1199–1217
Published online 15 March 2005 in Wiley InterScience (www.interscience.wiley.com). DOI: 10.1002/fld.959

Modelling of wetting and drying of shallow water using artificial porosity

B. van't Hof[‡] and E. A. H. Vollebregt[*,†]

VORtech, Industrial Computing, P.O. Box 260, 2600 AG Delft, The Netherlands

SUMMARY

A new method for wetting and drying in two-dimensional shallow water flow models is proposed. The method is closely related to the artificial porosity method used by different authors in Boussinesq-type models, but is further extended for use in a semi-implicit (ADI-type) time integration scheme. The method is implemented in the simulation model WAQUA using general boundary fitted coordinates and is applied to realistic schematization for a portion of the river Meuse in the Netherlands.

A large advantage of the artificial porosity method over traditionally used methods on the basis of 'screens' is a strongly reduced sensitivity of model results. Instead of blocking all water transport in grid points where the water level becomes small, as in screen-based methods, the flow is gradually closed off. Small changes in parameters such as the initial conditions or bottom topography therefore no longer lead to large changes in the model results. Copyright © 2005 John Wiley & Sons, Ltd.

KEY WORDS: shallow water equations; wetting and drying; artificial porosity method; sensitivity of model results

1. INTRODUCTION

Shallow water flow problems cover a wide range of practical problems, varying from the scale of oceans (storm surge prediction) to river sections or lakes. In various occasions the correct representation of wetting and drying is an important aspect. Of course this holds for dam and dike break problems and the corresponding flooding of initially dry land [1]. But wetting and drying are also relevant for simulation of rivers and coastal areas. They determine the retention surface through the wetting state of outer marches and banks, which consequently affect the propagation speed of flood waves and tidal waves. Various examples are given in References [2–4].

*Correspondence to: E. A. H. Vollebregt, VORtech, Industrial Computing, P.O. Box 260, 2600 AG Delft, The Netherlands.
†E-mail: edwin.vollebregt@vortech.nl
‡E-mail: bas.vanthof@vortech.nl

Contract/grant sponsor: Dutch National Institute for Coastal and Marine Management (Rijkswaterstaat/RIKZ)

Received 17 April 2004
Revised 7 December 2004
Accepted 31 January 2005

Figure 1. Illustration of screen-based wetting and drying methods for a part of the Meuse river in case of a flood wave due to heavy rainfall. Thick lines: weirs, model elements used to represent local strong bottom variations. Dashed lines: temporary screens placed to avoid flow at dry grid points.

Many numerical models for free surface shallow water flow in rivers, estuaries and coastal areas are based on staggered grids [2, 5–7]. In these methods drying and wetting are usually accounted for by placing 'thin dams' or 'screens' in velocity points of the grid when the water depth drops below a certain drying threshold, and removing the screens when the water depth rises again above a flooding threshold. When a screen is placed, the flow velocity is set to zero and the point is taken out of the computation. The different wetting and drying methods mainly differ in the criterions that are used for determining when a point becomes dry or is wetted again, see Reference [8] for an overview.

Screen-based approaches to wetting and drying have been thoroughly studied (Figure 1), and improvements have been made through the years [2, 9, 10]. However, a number of disadvantages still remain:

1. Because the grid points are excluded or included in the domain so abruptly, the drying and flooding processes cause extreme sensitivity to round-off errors. This sensitivity is illustrated by Figure 8, where round-off errors locally introduce differences in predicted water levels exceeding 25 cm.
2. Flooding takes place at a maximum speed of one grid point per time step. Inaccuracies occur when the actual flooding speed is greater.
3. In semi-implicit time integration schemes, the drying procedure must be intertwined with the iterative solution process for the water levels at a new time level. This complicates the analysis of the numerical method that is used.

An alternative approach to flooding and drying is proposed in References [11, 12] for Boussinesq-type models. It uses the notion of *artificial porosity* to allow a more gradual

transition between dry and wet grid points. The artificial porosity concept has been adapted for the use in the shallow water model WAQUA of the Dutch Rijkswaterstaat. The necessary adjustments mainly involved the incorporation of the method in the alternate direction implicit (ADI) time integrator and the solvers employed. The method is applied to several schematic test cases, and one real-life problem for an actual river section on a curvilinear grid. The simulation results obtained with the new approach are encouraging.

The remainder of this article is organized as follows. Section 2 discusses the idea of artificial porosity in terms of differential equations. Section 3 discusses the aspects of the discretization of the equations, as well as the solution procedure of the discrete equations. Section 4 shows our test results. Finally, some conclusions are drawn in Section 5.

2. SHALLOW WATER MODEL WITH ARTIFICIAL POROSITY

This section discusses the idea of artificial porosity in terms of differential equations. We present a simplified form of the shallow water equations (SWE), and introduce the traditional screen-based approach. Next the way in which the original SWE are modified is described so that the computational domain no longer varies with time. Some analyses of the modified (*artificially porous*) SWE are given: concerning the conservation of momentum and energy, and concerning a phenomenon which can be called *trickle flow*. This phenomenon only occurs in the artificially porous equations and not in the original SWE.

2.1. Shallow water equations

The two-dimensional depth-averaged shallow water flow equations are given by the continuity equation (1a) and the momentum equations in u- and v-directions (1b), (1c), see e.g. Reference [13].

$$\frac{\partial \zeta}{\partial t} + \frac{\partial Hu}{\partial x} + \frac{\partial Hv}{\partial y} = 0 \tag{1a}$$

$$\frac{\partial u}{\partial t} + u\frac{\partial u}{\partial x} + v\frac{\partial u}{\partial y} + g\frac{\partial \zeta}{\partial x} + \lambda u = 0 \tag{1b}$$

$$\frac{\partial v}{\partial t} + u\frac{\partial v}{\partial x} + v\frac{\partial v}{\partial y} + g\frac{\partial \zeta}{\partial y} + \lambda v = 0 \tag{1c}$$

where

$$H = H(\zeta + d) \tag{1d}$$

$$\lambda = g\sqrt{u^2 + v^2}/(C^2 H) \tag{1e}$$

Here the following symbols are used:

ζ water level, relative to a reference plane $z = 0$
d bottom depth below the reference plane (positive downwards)

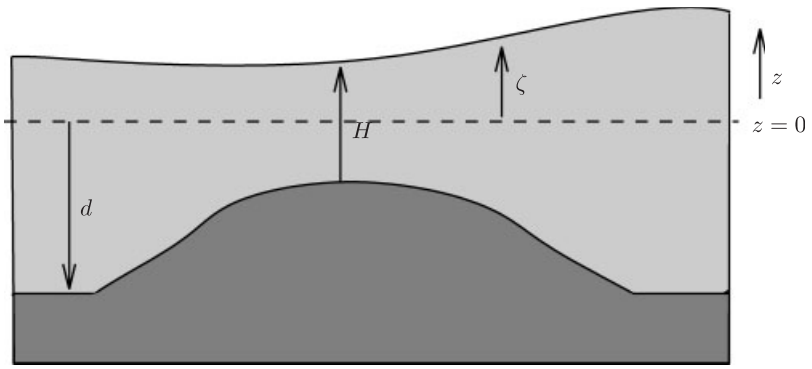

Figure 2. Illustration of the meaning of symbols ζ (water level), H (flow-through height) and d (bottom level), and the reference plane $z = 0$.

- H flow-through height, usually called water height above bottom level
- u, v components of the depth-averaged flow velocity
- g gravitational acceleration
- C Chézy-coefficient for bottom friction [14]

Some of the symbols are illustrated in Figure 2. All symbols are listed in the Nomenclature.

A number of phenomena that are not essential to the problem of wetting and drying have been omitted, e.g. the Coriolis force and influences of wind and turbulence.

Equations (1) are applied only in the wet part of the domain of interest. In the dry part, the flow velocity and the water level are meaningless, and any equation may be prescribed here, e.g. $u = v = 0$ and $\zeta = -d$. Due to rising and falling of the water level ζ, the domain of the equations varies in time. The problem to be solved is therefore a *moving boundary problem*.

The boundary equations to be applied at the boundary between the dry and wet parts of the domain remain a subject for research [13]. This paper is not concerned with this issue. The only goal is to find reliable solutions for the standard case, in which the boundary condition is $\zeta = -d$.

2.2. Traditional approaches for wetting and drying: using screens

In literature a vast amount of strategies can be found for simulation problems with moving boundaries, e.g. tracking where the front/boundary of the domain is on a fixed grid (surface markers), tracking fluid using markers (marker-and-cell method), tracking the fluid using an indicator function (volume-of-fluid and level-set methods), using moving coordinates (Lagrangian approach), stretching the grid near the interface, etc. An overview and references to many methods are presented in Reference [15].

The primary approach that is followed in shallow water simulation appears to be by marking grid cells or cell-faces as wet or dry on a fixed grid. For instance Balzano [8] discusses 10 varieties of this approach as presented by various authors in the field. We call these methods 'screen-based methods' because they can all be implemented using screens or thin dams at

appropriate locations, i.e. the velocity points of the grid, that obstruct the flow to/from grid cells that are considered dry.

Crucial aspects in screen-based methods are as follows:

- How the bottom topography in water level and velocity points are specified, e.g. the values in velocity points may be specified by the user, the values in water level points derived from this by various criteria (min, mean, max) [4].
- How the interpolation of water levels to velocity points is defined. The water level at the velocity point between water level points m and $m+1$ may for instance be calculated using arithmetic averaging ($\zeta_{m+1/2} = (\zeta_m + \zeta_{m+1})/2$), but also using an upwind approach or using other criteria.
- Which criteria are used for declaring cells or cell-faces wet or dry, e.g. checking against a flooding threshold δ, drying threshold $\delta/2$ (using a hysteresis to prevent flip-flop behaviour), or using tolerance 0 in other cases.
- At which positions in the solution algorithm the various checks are performed. For instance drying and flooding can be checked before starting the solution procedure for water levels at a new time step, within the solution procedure only drying is allowed to prevent infinite loops.

Even after long times of tuning and extension of these ideas, we still notice a number of problems that are inherent to the screen-based approach:

- The wetting strategy only removes screens at grid points adjacent to wet area. Therefore flooding never happens faster than one grid size per time step. This poses a time step restriction which cannot always be satisfied.
- The dry area never completely dries up. Typical values for the drying threshold are 1–15 cm, the latter of which implies a considerable amount of water being retained. In some cases even more water remains in 'dry' areas. For instance when removing a screen would lead to an unacceptably large flow within one time step, which would result in negative water heights.
- The wetting and drying procedure largely complicates the solution procedure for the shallow water problem. The various choices for the elements of screen-based methods presented above are strongly interrelated. This complexity makes it hard to analyse the properties of the overall numerical solution method (accuracy, stability, etc.). Further it is difficult to achieve the correct wetting and drying behaviour in all kinds of situations.
- The change of regimes between wet and dry is abrupt and is limited to the times corresponding to integer time steps. These sudden changes may introduce non-physical reflections, and also increase the sensitivity of the model results.

The sensitivity of model results was one of our main motivations for pursuing enhanced wetting and drying methods. The sensitivity problem can be formulated as follows:

> 'Even the smallest change anywhere in the model (geometry, coefficients, initial conditions, round-off errors) may introduce significant changes to the simulation results at later times at various locations in the model'.

An infamous cause of sensitivities are switches in the model, where a certain calculation is only carried out if ζ is larger than a certain value. This is particularly so for the screen-based

approaches: flow is possible when $H > \delta$, but is obstructed for $H \leqslant \delta$. The solution of the equations depends on the intermediate quantity H in a discontinuous way.

Sensitivities complicate the comparison of scenarios. Users of the simulation model often want to subtract two scenarios from each other to determine the effect of a modification in the model. However, the differences are often locally much larger than expected, due to sensitivity of the model. For instance when a screen at one location is placed one time step later in the first model run than in the latter one. Also more or less water may trapped in a grid cell by the surrounding screens in different model runs.

The sensitivity of model results further hampers performing regression tests. When the program is modified, the compiler may decide to rearrange computations. Simulations that should not be affected by the extensions can then still produce different results. The programmer then has to verify each time that the differences are 'normal' instead of due to programming faults.

Finally the sensitivity of model results is disadvantageous for the application of Kalman filtering. A Kalman filter has been implemented for the WAQUA model of Rijkswaterstaat and is able to significantly improve the storm surge prediction along the Dutch coast, e.g. reduce the RMS-error from 20 to 12 cm [16]. Because the SWE are slightly nonlinear, so-called 'error modes' (disturbances of the model state) are propagated using a linearization step that involves subtracting two scenarios. This is of course complicated when the sensitivity of a model is large.

In the following section, a fixed grid approach is introduced that does not require a strict differentiation between wet and dry cells, and so avoids the problems mentioned.

2.3. The new approach using artificial porosity

In numerical approximation, special precautions are taken to avoid that the water level ζ becomes lower than the bottom level $-d$, which would result in negative water volume at the given grid point.

One key element of the artificial porosity method is the introduction of the *pseudo-water level* ψ. The pseudo-water level is allowed to freely drop below the bottom as illustrated in Figure 3. It replaces the true water level ζ in most places in the equations. For instance it is used to approximate the water level gradient at the moving boundary.

The second key element of the artificial porosity method is to use a more gradual transition between 'wet' and 'dry' regimes. This is achieved through the definition of the flow-through height H, which is now defined by some function $H = H_\delta(\psi + d)$, depending on the threshold value δ. Different positive functions may be used. Kennedy *et al.* [11] and Madsen *et al.* [12] choose a function that is only defined if the pseudo-water level is high enough, i.e. $\psi + d \geqslant -D$ for some value D. For the purpose of robustness, we have used a function that is defined for all $\psi + d$ as shown in Equation (2).

$$H = H_\delta(\psi + d) = \begin{cases} \psi + d & \text{if } \psi + d \geqslant \delta \\ \delta^2/(2\delta - (\psi + d)) & \text{if } \psi + d < \delta \end{cases} \tag{2}$$

This function has been chosen such that the flow-through height is equal to the original one when $\psi + d > \delta$, and that the flow-through height tends to zero for negative $\psi + d$. Since the flow-through height is never zero or below, the computational area of the problem never changes: the artificially porous problem lives on the entire grid.

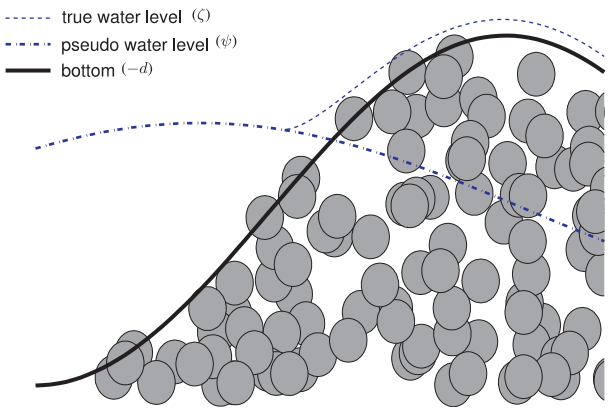

Figure 3. The artificial porosity approach. There are two water level fields: the *pseudo-water level* ψ and the *true water level* $\zeta = H - d$.

Finally, the 'true' water level ζ that is computed by the program is defined such that it easily displays the volume of water in grid cells:

$$\zeta = -d + H_\delta(\psi + d) \tag{3}$$

The modified SWE read:

$$\frac{\partial \zeta}{\partial t} + \frac{\partial Hu}{\partial x} + \frac{\partial Hv}{\partial y} = 0 \tag{4a}$$

$$\frac{\partial u}{\partial t} + u\frac{\partial u}{\partial x} + v\frac{\partial u}{\partial y} + g\frac{\partial \psi}{\partial x} + \lambda u = 0 \tag{4b}$$

$$\frac{\partial v}{\partial t} + u\frac{\partial v}{\partial x} + v\frac{\partial v}{\partial y} + g\frac{\partial \psi}{\partial y} + \lambda v = 0 \tag{4c}$$

For very small values of the threshold δ, the equations in the wet part of the domain are exactly the original SWE. In the dry part of the domain, the equations $u = v = H = 0$ are no longer used. Instead, equations are used which are very similar to the original momentum and continuity equations. Some of the problems associated with the traditional 'screen' methods are avoided by the artificial porosity approach:

- The drying/wetting strategy is considerably simplified.
- Since drying/wetting is a much more gradual process, the sensitivity of the solutions is greatly reduced.
- Flooding may occur at greater speed than one grid size per time step.

2.4. *Conservation properties*

The momentum and continuity equations may be combined to derive the conservation laws for mass, momentum and energy. These conservation laws explain the local variations of mass,

momentum and energy in terms of fluxes and sources/sinks:

- *mass* is only subject to a transport term, called *discharge*;
- *momentum* is subject to three transport terms: advection, viscosity and (hydrostatic) pressure. Momentum source/sink terms come from friction, wind and the momentum exchange between the earth and the water at the bottom;
- *energy* is subject to two transport terms: advection and viscosity. Energy source/sink terms are wind, viscosity and friction.

Artificial porosity does not fundamentally change the conservation laws. Two terms, however, change when artificial porosity is included in the equations:

- Momentum transport due to the *pressure*-gradient changes. This term is equal to $\nabla(\frac{1}{2}g(\zeta+d)^2)$ in the original equations, but changes to

$$\nabla\left(\frac{1}{2}g(\psi+d)^2 - g\int_{\psi+d}^{\delta}(H_\delta(z)-z)\,\mathrm{d}z\right) \tag{5}$$

  in the artificially porous model.
  The original and artificially porous pressures are equal when the water height is more than the threshold δ. When the water height is below the threshold value, the artificially porous pressure is less than the original pressure. The porous approach can therefore also be understood as the introduction of a *suction force* where the water height is small.
- The expression for the *potential energy* changes. In the original equations, the potential energy is $He_\mathrm{p} = (g/2)(\zeta^2 - d^2)$. In the artificially porous model, it changes to $He_\mathrm{p} = g\int^{\psi} zH'_\delta(z+d)\,\mathrm{d}z$.
  The original and artificially porous potential energies are equal when the water height is more than the threshold δ. When the water height is below the threshold value, the artificially porous potential energy is more than the original potential energy.

Besides the two differences mentioned above, there is another difference: mass, momentum and energy can be transported across dry land in the artificially porous equations, which they cannot in the original equations. The amount of transport into and across the dry parts of the domain may be limited by the choice of the threshold δ, as is discussed in the following section.

2.5. *Trickle flow*

There is a qualitative difference between the solutions obtained with the artificial porosity approach and those obtained without it. It is illustrated in Figure 4: obstacles in the bottom profile no longer completely keep the water from flowing through. When a simulation is carried out long enough, any amount of water may therefore have passed through the obstacle in the computational domain.

In this section, it will be discussed how much water may pass through an obstacle, offering some insight in the effects of parameter settings (such as the choice of the threshold value δ).

In the dry part of the domain where $\psi+d<0$, the momentum equation will be dominated by the friction force, which will be in balance with the gravitational force. In the one-dimensional

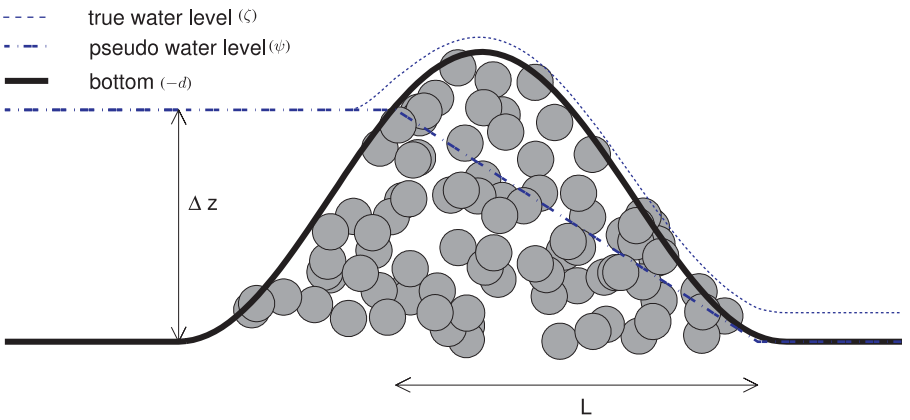

Figure 4. When artificial porosity is used to model drying and flooding, the water may flow (*trickle*) through obstacles, since the water height is never zero. After a long period of time, the water level at the left of the obstacle may therefore become equal to that at its right.

case this gives

$$g\frac{\partial \psi}{\partial x} + \frac{gu|u|}{C^2 H} = 0 \tag{6}$$

This equation can be integrated. The discharge Hu will be constant.

$$Hu = \left(\frac{1}{L}\int_L C^2 H^3 \frac{\partial \psi}{\partial x}\,\mathrm{d}x\right)^{1/2} = CH^{3/2}\sqrt{\Delta\psi/L} \tag{7}$$

for a value of C and H found in the interval L. The value of the Chézy parameter C often depends on the water height H. For instance the Manning formula [14] can be used which is given by

$$C = H^{1/6}/\eta \tag{8}$$

where η denotes Manning's coefficient. In this case the discharge Hu in (7) is given by

$$\begin{aligned} Hu &= \frac{1}{\eta}H^{5/3}\sqrt{\Delta\psi/L} \\ &= \frac{1}{\eta}\left(\frac{-\delta^2}{\psi + d - 2\delta}\right)^{5/3}\sqrt{\Delta\psi/L} \\ &= \mathcal{O}(|\psi + d|^{-5/3}\delta^{10/3}\sqrt{\Delta\psi/L}) \end{aligned} \tag{9}$$

Approximation (9) for the discharge shows the factors on which the strength of the 'trickle flow' depends:

1. The threshold value δ: if the threshold is 23% smaller, it lets half as much water trickle through.
2. The distance between the pseudo-water level and the bottom (i.e. the height of the obstacle): an obstacle that is 33% times taller lets half as much water trickle through.
3. The difference in water level at both ends of the obstacle: a water level difference that is four times larger lets twice as much water trickle through.
4. The width of the obstacle: an obstacle that is four times as wide lets half as much water trickle through.

Tests to quantify the trickle effect are described in Section 4.2. One typical result is that it leads to a discharge of $Hu = 0.02\ \mathrm{m}^2/\mathrm{s}$ for a water level difference $\Delta\psi = 5\ \mathrm{m}$ and threshold value $\delta = 0.1$.

3. DISCRETIZATION AND SOLUTION PROCEDURE OF THE SHALLOW WATER EQUATIONS

This section first discusses the aspects of the space and time discretization of the SWE, as used in the WAQUA package. A form of alternate direction implicit time integration (ADI) is used. Then the methods used for the solution of the discrete equations are described. Special attention is paid to the adjustments that were necessary for incorporating artificial porosity.

3.1. Space discretization of the shallow water equations

The WAQUA package uses an orthogonal curvilinear grid as illustrated in Figure 1. As can be seen, the curvilinear grid is designed to fit the geometry, choosing smaller mesh sizes in the locations where the solution fluctuates strongly. The orthogonality of the grid is used to avoid over-complicating the momentum equations in the curvilinear coordinates.

A staggered grid convention is used [13], in which the water levels and velocity vector components are approximated in different locations. The staggered grid avoids de-coupling of the solutions, which may cause non-physical wiggles in non-staggered grids. The type of grid used is the Arakawa C-grid where water levels are approximated in cell centres denoted by (i, j), u-velocities at vertical cell-faces $(i + 1/2, j)$ and v-velocities at horizontal cell-faces $(i, j + 1/2)$. The components of the flow velocity vector in terms of which the equations are stated are grid aligned, which means that they point in the grid directions. Since the grid is curvilinear, these directions vary throughout the grid.

Higher order upwind discretizations are combined with central discretization formulas for the advection terms in the momentum equation. The result is a discretization that produces very little wiggles and has very little artificial viscosity at the same time [7]. The discretizations used are mass conserving. Mass is conserved by defining the mass transport fluxes (discharges) Hu in the intermediate grid points $(i + 1/2, j)$ and the discharges Hv in the grid points $(i, j + 1/2)$, and using these in the mass balance

$$\Delta x_{ij}\Delta y_{ij}\frac{\partial \zeta_{i,j}}{\partial t} = \{\Delta yHu\}_{i+(1/2),j} - \{\Delta yHu\}_{i-(1/2),j} + \{\Delta xHv\}_{i,j+(1/2)} - \{\Delta xHv\}_{i,j-(1/2)} \quad (10)$$

3.2. Time integration of shallow water equations using ADI

Much of the work in the implementation of the artificial porosity method for the modelling of drying and flooding, was the integration of the porosity equations into the ADI-time integration scheme used by the WAQUA code [7].

The ADI-scheme calculates the water levels and flow velocities at the time level $t+1$ from those at the time level t in four steps. The main structure of the calculation is discussed below. The introduction of the artificial porosity approximation of the water height is discussed in Section 3.4.

- First half time step:
  - Momentum equation in v-direction
    The first step in the computation involves the solution of the momentum equation in the v-direction for a half time step. The only variable that changes is the v-velocity: the u-velocity and the water levels remain unchanged.
    The variable v is used mostly at the new time level $t+\frac{1}{2}$ for the terms in the momentum equation. A frozen coefficient approach is used to make the system linear. The resulting momentum equation is:

$$\frac{v^{t+(1/2)}}{\Delta t/2} + v^t \frac{\partial v^{t+(1/2)}}{\partial y} + u^t \frac{\partial v^{t+(1/2)}}{\partial x} + \lambda^t v^{t+(1/2)} = \frac{v^t}{\Delta t/2} - g\frac{\partial \psi^t}{\partial y} \tag{11}$$

    The equation is a linear system. A line Gauss–Seidel iteration method is used for the solution of the system. No major adjustments have been made to the original WAQUA code.
  - Coupled continuity and momentum equations
    The second step in the computation is a coupled system of the continuity equation and the momentum equation in the u-direction. The water levels are taken at the new time level $t+\frac{1}{2}$. The u-velocity is taken at the new time level in a small number of terms. The result is a number of independent systems of equations, in which there is only a coupling of the unknowns in the x-direction. The system is linear in the u-velocities, and nonlinear in the water levels. The solution is found by successive linearization (using frozen coefficients) and direct solution of the resulting tridiagonal linear systems.
    The system is given by

$$\frac{\zeta^{t+(1/2)}}{\Delta t/2} + \frac{\partial}{\partial x} H^{t+(1/2)} u^{t+(1/2)} = \frac{\zeta^t}{\Delta t/2} - \frac{\partial}{\partial y} H^t v^t \tag{12}$$

$$\frac{u^{t+(1/2)}}{\Delta t/2} + u^{t+(1/2)} \frac{\partial u^t}{\partial x} + g\frac{\partial \psi^{t+(1/2)}}{\partial x} + \lambda^t u^{t+(1/2)} = \frac{u^t}{\Delta t/2} - v^{t+(1/2)} \frac{\partial u^t}{\partial y} \tag{13}$$

- Second half time step:
  - Momentum equation in u-direction
    The third step in the computation is the solution of the momentum equation in the u-direction for the second half of the time step. This step is very similar to the first

step in the calculation.

$$\frac{u^{t+1}}{\Delta t/2} + u^{t+(1/2)}\frac{\partial u^{t+1}}{\partial x} + v^{t+(1/2)}\frac{\partial u^{t+1}}{\partial y} + \lambda^t u^{t+1} = -\frac{u^{t+(1/2)}}{\Delta t/2} - g\frac{\partial \psi^{t+(1/2)}}{\partial x} \tag{14}$$

- Coupled continuity and momentum equations
  The last step in the computation is a coupled system like the second step.

$$\frac{\zeta^{t+1}}{\Delta t/2} + \frac{\partial}{\partial y}H^{t+1}v^{t+1} = \frac{\zeta^{t+(1/2)}}{\Delta t/2} - \frac{\partial}{\partial x}H^{t+(1/2)}u^{t+(1/2)} \tag{15}$$

$$\frac{v^{t+1}}{\Delta t/2} + v^{t+1}\frac{\partial v^{t+(1/2)}}{\partial y} + g\frac{\partial \psi^{t+1}}{\partial y} + \lambda^t v^{t+1} = \frac{v^{t+(1/2)}}{\Delta t/2} - u^{t+1}\frac{\partial v^{t+(1/2)}}{\partial y} \tag{16}$$

Since all the terms appear as an implicit term in one of the time step halves, and as an explicit term in the other, the resulting time integration method is second order accurate and (theoretically) unconditionally stable.

3.3. Solution method of the original WAQUA code

The momentum equations (11) and (14) are linear systems and can be solved using Gauss–Seidel iteration.

The coupled equations (12), (13) and (15), (16) are nonlinear. The momentum equations (13) and (16) are linear, but the continuity equations (12) and (15) are quadratic. Successive Picard linearization is used for solving these systems.

In the original WAQUA code, the water height H is checked before the iterative solution procedure starts. Screens are removed at velocity points where sufficient water is found.

Next, the water height H is also checked at every iteration. Velocity grid points where the water height is negative are taken out of the simulation domain by setting the velocity to zero. If a negative water height is found at a water level grid point, all the velocity grid points around the given water level grid point are taken out of the computational domain.

Screens are only removed before the solution procedure and only added during the iterations, which ensures that a solution will be found.

3.4. Solution of the artificially porous system

The introduction of the artificial porosity approximation for the water height introduces no changes in the parts of the code that solve the momentum equations only (steps 1 and 3).

The introduction of artificial porosity somewhat complicates the solution procedure for the continuity equations (12) and (15) for two different reasons.

The first reason is that it must be made sure that systems (12) and (15) really have a solution. In case of 'over-draining' (see Section 3.5), this may not be the case, so some adjustments need to be made to the system to give it a solution.

The second reason is that in the case of the artificially porous equations, systems (12) and (15) are no longer quadratic, since the function H_δ (2) is used. A suitable linearization is to be chosen for the solution procedure of the system.

The structure of the discrete system, of which the semi-discrete formulation is given in (13), (12) can be clarified by lumping all the right hand sides, and omitting all the

time-subscripts for the new time level $t + \frac{1}{2}$. The system then becomes:

$$\frac{\zeta_{ij}}{\Delta t/2} + \frac{H_{i+(1/2),j}u_{i+(1/2),j}\Delta y_{i+(1/2),j} - H_{i-(1/2),j}u_{i-(1/2),j}\Delta y_{i-(1/2),j}}{\Delta x_{ij}\Delta y_{ij}} = \mathrm{RHS}_{ij}$$

$$\left(\frac{1}{\Delta t/2} + \lambda_{i+(1/2),j} + \frac{\partial u^t}{\partial x}\right) u_{i+(1/2),j} + g\frac{\psi_{i+1,j} - \psi_{ij}}{\Delta x_{i+(1/2),j}} = \mathrm{RHS}_{i+(1/2),j} \quad (17)$$

with the right-hand sides RHS_{ij} and RHS_{ij} given by

$$\mathrm{RHS}_{ij} = \frac{H^t}{\Delta t/2} + \frac{\partial}{\partial y}H^t v^t$$

$$\mathrm{RHS}_{i+(1/2),j} = \frac{u^t}{\Delta t/2} - v^{t+(1/2)}\frac{\partial u^t}{\partial y} \quad (18)$$

An iterative scheme is used for the solution of system (17). The system is made linear in every iteration level q by a frozen coefficient approach for all the terms except the water height $H^{[q+1]}$ at the new iteration level. For this term the following linearization is used:

$$\tilde{H}^{[q+1]} = H^{[q]} + (\psi^{[q+1]} - \psi^{[q]}) \cdot H'_\delta(\psi^{[q]} + d) \quad (19)$$

The linear system that is solved in every iteration is given by

$$\frac{\tilde{H}_{ij}^{[q+1]} - d_{ij}}{\Delta t/2} + \frac{H_{i+(1/2),j}^{[q]}u_{i+(1/2),j}^{[q+1]}\Delta y_{i+(1/2),j} - H_{i-(1/2),j}^{[q]}u_{i-(1/2),j}^{[q+1]}\Delta y_{i-(1/2),j}}{\Delta x_{ij}\Delta y_{ij}} = \mathrm{RHS}_{ij} \quad (20a)$$

$$\left(\frac{1}{\Delta t/2} + \lambda_{i+(1/2),j} + \frac{\partial u^t}{\partial x}\right) u_{i+(1/2),j}^{[q+1]} + g\frac{\psi_{i+1,j}^{[q+1]} - \psi_{ij}^{[q+1]}}{\Delta x_{i+(1/2),j}} = \mathrm{RHS}_{i+(1/2),j} \quad (20b)$$

The linear momentum equation (20b) is substituted into the linearized continuity equation (20a). The result is a number of independent tridiagonal systems for the pseudo-water levels $\psi^{[q+1]}$. These systems can be solved directly using a double sweep, after which the next iteration can be done.

3.5. *Over-draining*

In the ADI-method for time integration presented in Section 3.2, an explicit approximation is used for the discharges Hv in the first half of the time step (12) and for the discharges Hu in the second half (15).

There is no guarantee that these explicit fluxes do not extract more water from a row or column of control volumes than is stored in the entire row or column. Such a situation is called 'over-draining' of a grid row or column. When over-draining occurs, system (12) or (15) has no solution.

To avoid over-draining, the explicit discharges are limited so that they do not extract more than 90% of the available water volume from any control volume. One needs to proceed with care when limiting the discharges, because, obviously, any extracting water from a control

volume supplies water to another control volume. Therefore, limiting the discharge from an over-drained control volume may cause over-draining in the neighbouring control volume. An iterative procedure is used to obtain the correct explicit discharges: in every iteration, the set of over-drained control volumes is extended. The water-extracting discharges are limited for every over-drained control volume just so much, that exactly 10% of the water remains (this requires the solution of a tridiagonal linear system for all over-drained control volumes). The iteration procedure finishes when an iteration does not cause any new control volumes to over-drain.

The discharges will only be limited if over-draining is about to occur. In a rectilinear grid, this happens when

$$\Delta t > 0.9 \frac{H}{\partial Hv/\partial y} \tag{21}$$

Note that this is a grid-independent time step limit. Loss of accuracy may occur if the discharges need to be limited.

In the tests presented in Section 4, over-draining hardly ever occurs. The treatment for over-draining discussed in this section has been tested in other tests, in which the correctness of the implementation was determined.

3.6. The option 'quantify randomness'

In the course of this research a new option has been developed for WAQUA to investigate the sensitivity of a scenario. This new option is called 'quantify randomness'. It clearly shows the effects that small disturbances and round-off errors during the simulation may have on the simulation results.

The option works by implementing two equivalent versions for one key operation in the solution algorithm. In WAQUA this key step is chosen to be the double sweep algorithm for solving tridiagonal systems of equations for the new water levels. In the original implementation these systems are solved by a forward sweep, eliminating the lower diagonal, and a backward sweep, solving the system by back-substitution. The second implementation consists of performing a backward sweep, eliminating the upper diagonal, and a forward sweep for back-substitution.

These two implementations are completely equivalent. There is not one single argument why one of the algorithms should produce 'better' results than the other. In the presence of round-off error they however produce different results. These differences are introduced in every time step of the simulation and throughout the model. The differences of previous time steps propagate through the model and may trigger other behaviour of the model, for instance trigger differences in the drying and flooding procedures.

The procedure to determine the sensitivity of a scenario now consists of running the simulation with both implementations and comparing the results. Although there is no guarantee that this difference is anywhere near the actual difference to the exact solution, the option still gives a very valuable first guess. In practice the pattern and size of the differences between the two runs appears to be well comparable to differences obtained through other means: comparing a sequential to a parallel run, with/without compiler optimizations, etc. Therefore it helps well in judging the results of regression tests: distinguishing programming faults from the inherent behaviour of a scenario.

4. RESULTS

This section shows results that are obtained with the new wetting and drying method. First schematic test-cases are used to show the effects of the artificial porosity approach and to analyse the trickle effect that was described in Section 2.5. Then the results are shown for a realistic model of a part of the Meuse river. The sensitivity of the model results to small changes (such as round-off errors) turns out to be greatly reduced by the new wetting and drying model.

4.1. One-dimensional test-case

The effects of artificial porosity for a simulation in which drying and flooding occur is shown in a simple one-dimensional test. The domain is shown in Figure 5: the bottom is a slope. At the open boundary at the left, the water level is prescribed as a boundary condition. The water level drops slowly, so that the water is drained gradually from the domain. After most of the water has been drained, the water level boundary condition is increased fast. The domain floods again.

The simulation results are shown in Figure 6. When using small time steps, the solutions obtained with screens are almost identical to those obtained with artificial porosity. When a larger time step is used, however, flooding can only occur at a rate of one grid size per time step. Artificial porosity avoids this problem.

4.2. Magnitude of the trickle effect

A second test is used to quantify the trickle effect (see Section 2.5). For this a simple canal is used with a single obstacle of one mesh width in the middle. The canal is 10 000 m long and is discretized with mesh widths $5\,\mathrm{m} \leqslant \Delta x \leqslant 500\,\mathrm{m}$.

In a simple test with $L = 20\,\mathrm{m}$ and $\Delta z = 4\,\mathrm{m}$ (see Figure 4), the mesh size and the threshold depth were varied. The results are shown in Table I. All values found are negligible.

4.3. Detailed model of the Meuse river

A real-life test case contains a part of the Meuse river in the south of the Netherlands. The simulation domain is approximately 7 km long and 2 km wide, and the curvilinear grid consists of 200×50 grid points, resulting in a grid size of approximately 40 m. The time step used is 15 s. The flooding threshold δ was 1 cm.

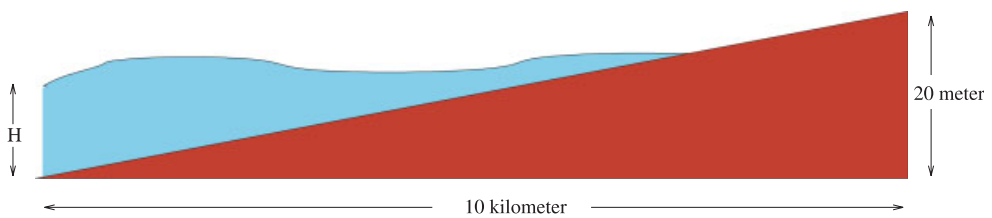

Figure 5. The domain in the one-dimensional test (depth-averaged calculation).

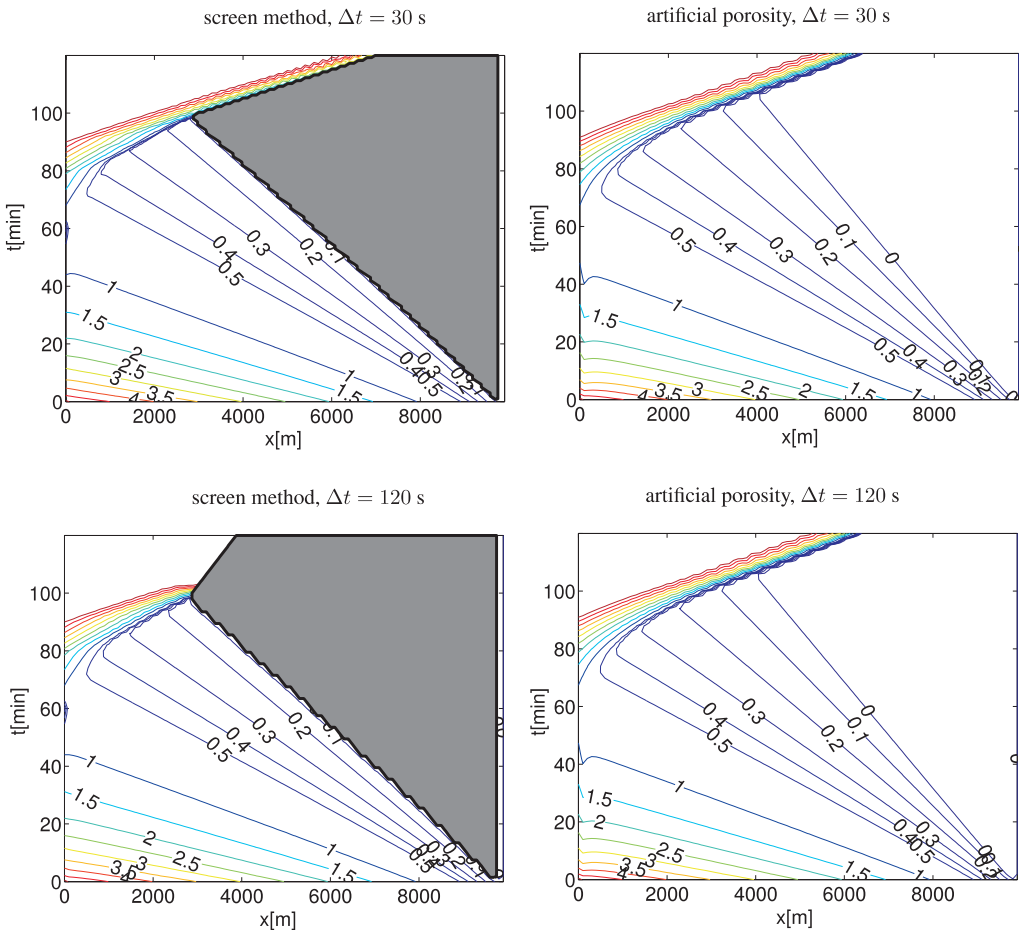

Figure 6. Contours of pseudo-water heights $\psi + d$ in the one-dimensional test problem. The results are shown in time-location format (note the axes). Left: the dry land is coloured grey. Apparently, the land is considered dry when the water height drops below 10 cm. Flooding occurs at a maximum speed of one grid size per time step. Right: the artificial porosity approach avoids this problem.

Table I. Discharge per unit of width (Hu) due to trickle flow as function of the parameters of the trickle test.

	$\delta = 0.2$ m	$\delta = 0.1$ m	$\delta = 0.05$ m
$\Delta x = 20$ m	0.021 m^2/s	0.006 m^2/s	0.0014 m^2/s
$\Delta x = 10$ m	0.051 m^2/s	0.010 m^2/s	0.0025 m^2/s
$\Delta x = 5$ m	0.070 m^2/s	0.016 m^2/s	0.004 m^2/s
$\Delta x = 2.5$ m	0.080 m^2/s	0.020 m^2/s	0.004 m^2/s

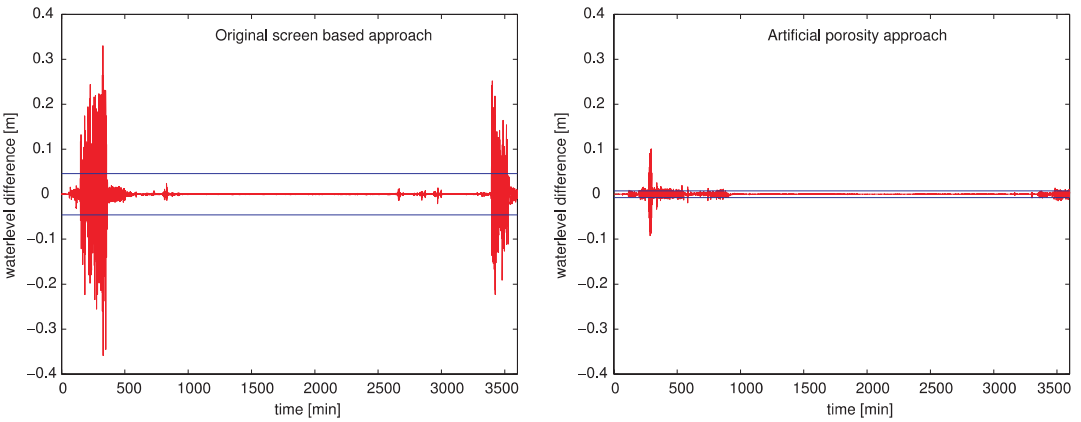

Figure 7. Water level difference due to round-offs at one location in the Meuse model (marked by circles in Figure 8) as a function of time. Differences in rounding errors between two otherwise identical runs lead to significant differences in the simulation results. The value that is exceeded in 5% of the times (95%-quantile) is marked with two horizontal lines.

In a simulation used to assess the risk of flooding after severe rainfall, the discharge at the entrance of this part of the Meuse (south in the model) is increased, over a period of 24 h, from 250 to 3000 m^3/s. The discharge is then kept constant for 12 h, after which it is reduced to its original level in the course of another 24 h.

Most of the domain is flooded during the simulation, after which a large part of the domain (but not the entire domain) becomes dry again. These results are computed more or less identically by both the original screens method and the new method based on artificial porosity.

Due to various reasons the simulation results for this model are sensitive to small disturbances. This is awkward for users of the model, for instance when comparing two scenarios. The sensitivities are caused among others by the wetting and drying methods used.

The sensitivity of the model is quantified with the option quantify randomness as explained in Section 3.6. The differences between the simulation results for the two runs are unexpectedly large, as illustrated in Figure 7. The top-left figure shows a time-series of the difference in one location for the original simulation method. The difference displays a more or less chaotic behaviour. In order to quantify the magnitude of the noise we select the largest value that occurs at least 5% of the time. This '95%-quantile' is shown in the figure by the horizontal lines. In 5% of the times the absolute value of the difference exceeds this line. For the original simulation method the sensitivity in this point is thus quantified as 4.6 cm.

The top-right graph in Figure 8 shows the results for the same location, but now with the artificial porosity method. In this case the 95%-quantile is found at 7 mm, i.e. the sensitivity is strongly reduced.

Finally the bottom two graphs display the sensitivity values for the entire simulation domain. It can easily be seen that the sensitivity is significantly reduced. Where the values are typically 10 cm in the lower part of the domain when the screens method is used, they rarely exceed 1 cm when the artificial porosity method is used.

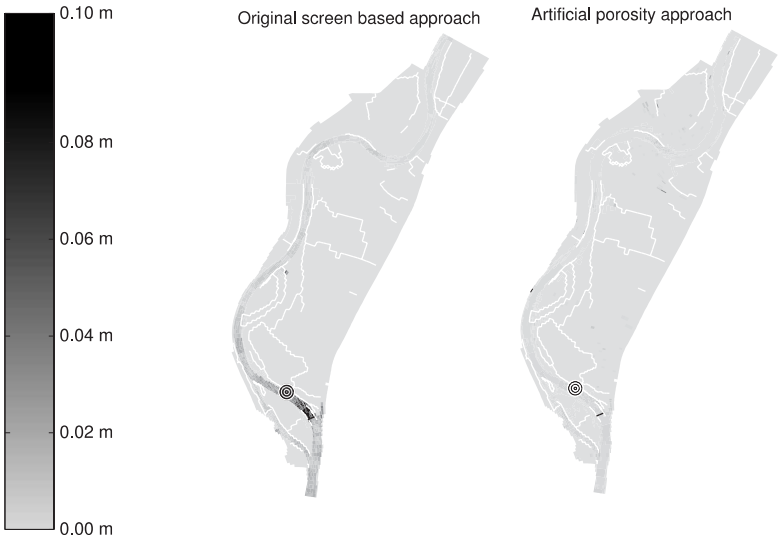

Figure 8. Sensitivity statistics for the Meuse model. The value that is exceeded 5% of the time (95%-quantile, [m], illustrated for one location in Figure 7) is calculated at every grid point. At many locations, this value is 10 cm or more in the screen approach. It is a lot smaller in the artificial porosity approach.

5. CONCLUSIONS

In this paper a new method is presented for the numerical treatment of the moving land–water boundary in shallow water models. The method consists of a slight extension to the SWE themselves, i.e. the introduction of the pseudo-water level ψ that is allowed to drop below the bottom level. This extension makes that no longer a distinction has to be made between wet and dry land; the same equations are applied throughout the entire simulation domain. This eliminates the need for all kinds of ad hoc criteria for determining the flow status of grid points that complicate the model and program code.

The simulation results differ very little from those obtained with traditional screen-based methods, except that the solutions are much less sensitive to small perturbations such as round-off errors. This is achieved by avoiding the abrupt changes from wet to dry of the traditional methods. Moreover some artifacts are avoided, such as the water that is sometimes trapped in dry areas of the simulation domain. This together simplifies the comparison of scenarios and thus enhances the user-friendliness and applicability of the model.

NOMENCLATURE

ζ	water level (m)
ψ	pseudo-water level (m)
d	bottom depth (m)
H	water height (m)
L	characteristic (horizontal) distance (m)

δ flooding threshold (m)
u flow velocity in x-direction (m/s)
v flow velocity in y-direction (m/s)
g gravitational acceleration (m/s^2)
C Chézy parameter ($\sqrt{m}/s$)
λ friction parameter (1/s)
e_p density of potential energy (J/m^3)

ACKNOWLEDGEMENTS

Thanks to the Dutch National Institute for Coastal and Marine Management (Rijkswaterstaat/RIKZ), for the use of their software.

REFERENCES

1. Stelling GS, Duynmeyer SPA. A staggered conservative scheme for very Froude number in rapidly varied shallow water flows. *International Journal for Numerical Methods in Fluids* 2003; **43**:1329–1354.
2. Falconer RA, Owens PH. Numerical simulation of flooding and drying in a depth-averaged tidal flow model. *Proceedings of the Institution of Civil Engineers-Civil Engineering* 1987; **83**:161.
3. Molinaro P, Di Filippo A, Ferrari F. Modelling of flood wave propagation over flat dry areas of complex topography in presence of different infrastructures. In *Proceedings of the Specialty Conference on Modelling of Flood Propagation Over Initially Dry Areas*, ASCE (eds), ASCE: New York, 1994; 209–228.
4. Stelling GS, Wiersma AK, Willemse JBTM. Practical aspects of accurate tidal computations. *Journal of Hydraulic Engineering* (ASCE) 1986; **112**:802–817.
5. Casulli V. Semi-implicit finite difference methods for the two dimensional shallow water equations. *Journal of Computational Physics* 1990; **86**:56–74.
6. Leendertse JJ. Aspects of a computational model for long period water wave propagation. *Technical Report RM-5294-PR*, Rand Corporation, Santa Monica, CA, 1967.
7. Stelling GS. On the construction of computational methods for shallow water flow problems. *Ph.D. Thesis*, Delft University of Technology, 1983.
8. Balzano A. Evaluation of methods for numerical simulation of wetting and drying in shallow water flow models. *Coastal Engineering* 1998; **34**:83–107.
9. van Kester JAThM, de Goede ED. Verbeteren van algoritme voor droogvallen en onderlopen in WAQUA en TRIWAQ. *Technical Report Z2292*, Delft Hydraulics, The Netherlands, 1997.
10. Vollebregt EAH, van Kester JAThM. Inventarisatie van problemen en oplosrichtingen m.b.t. droogvallen en onderlopen in WAQUA en TRIWAQ. *Technical Report TR02-13*, VORtech, P.O. Box 260, 2600 AG Delft, The Netherlands, November 2002.
11. Andrew B, Kennedy, Qin Chen, James T Kirby. Boussinesq modeling of wave transformation, breaking and runup. I: 1D. *Journal of Waterway, Port, Coastal, and Ocean Engineering* 2000; 39–47.
12. Madsen PA, Sørensen OR, Schäffer HA. Surf zone dynamics simulated by a boussinesq type model. Part I. Model description and cross-shore motion of regular waves. *Coastal Engineering* 1997; **32**:255–287.
13. Vreugdenhil CB. *Numerical Methods for Shallow-Water Flow, Water Science and Technology Library*, vol. 13. Kluwer Academic Publishers: Dordrecht, The Netherlands, 1994.
14. Chow VT. *Open Channel Hydraulics*. McGraw-Hill: New York, 1959.
15. Scardovelli R, Zaleski S. Direct numerical simulation of free-surface and interfacial flow. *Annual Reviews of Fluid Mechanics* 1999; **31**:567–603.
16. de Vries JW. Verification of the WAQUA/CSM-16 model for the winters 1992/1993 and 1993/1994. *Technical Report TR-176*, KNMI, 1995.

